Variability in Heart-to-Mediastinum Ratio from Planar ^{123}I-MIBG Images of a Thorax Phantom for 6 Common γ-Camera Models

Rikard Owenius[1], Michelle Zanette[2], and Patrick Cella[2]

[1]*Department of Surgical Sciences, Radiology, Uppsala University, Uppsala, Sweden; and* [2]*GE Healthcare, Life Sciences, Imaging R&D, Marlborough, Massachusetts*

A heart-to-mediastinum (H/M) ratio of 1.6 or greater on planar ^{123}I-iobenguane (^{123}I-MIBG) images identifies heart failure patients at low risk of experiencing an adverse cardiac event. This phase-4 study used standardized phantoms to assess the intercamera, intracamera, and interhead variability in H/M ratio determinations from planar cardiac ^{123}I-MIBG imaging using commercially available, dual-head γ-cameras. **Methods:** A fillable thorax phantom was developed to simulate the typical uptake of ^{123}I-MIBG. The phantom had a nominal H/M ratio of 1.6 on the reference camera. Commercial cameras used in the study were dual-head and capable of 90° configuration for cardiac imaging. The target sample size was 8 units (examples) per camera model. Two imaging technologists independently analyzed planar images of simulated ^{123}I-MIBG uptake from the thorax phantom. H/M was the ratio of the average counts per pixel of the heart and mediastinum regions of interest. The primary endpoint, intercamera variability in H/M ratio from head 1, was determined for each camera model via comparison with the H/M ratio on the reference camera. Only cameras with at least 8 units tested ($n \geq 8$) were included in the primary analysis. Intracamera and interhead variability in the H/M ratio were also evaluated. **Results:** Nine camera models were studied. The mean H/M ratio ranged from 1.342 to 1.677. The primary analysis (6 camera models) using a mixed-model, repeated-measures analysis showed no significant difference in H/M ratio between any camera model and the reference camera. Intracamera variability (head 1) in the H/M ratio among camera models with 8 units or more was high, with SDs ranging from 0.0455 to 0.1193. Interhead variability was low (SDs of the interhead difference, 0.017–0.074). **Conclusion:** Commonly used γ-cameras produced H/M ratios from simulated ^{123}I-MIBG phantom images that were not significantly different from those on the reference camera. This finding indicates that the results of previous clinical trials of ^{123}I-MIBG, involving many different clinical sites and camera models, are valid. The assessment of the performance of a given camera unit using an ^{123}I planar phantom before H/M results from ^{123}I-MIBG imaging are used for classifying risk in heart failure patients is encouraged.

Key Words: iobenguane; MIBG; phantom; heart-to-mediastinum ratio; heart failure

J Nucl Med Technol 2017; 45:297–303
DOI: 10.2967/jnmt.117.196055

Heart-to-mediastinum (H/M) ratio on planar ^{123}I-iobenguane (^{123}I-MIBG) images is a prognostically useful measure of myocardial sympathetic innervation in patients with heart failure that can identify patients at low risk of all-cause and cardiac mortality at 1 and 2 y. In the ADMIRE-HF (AdreView Myocardial Imaging for Risk Evaluation in Heart Failure) study, subjects with an H/M ratio of less than 1.6 were at higher risk of experiencing an adverse cardiac event than subjects with an H/M ratio 1.6 or greater. Similar results were obtained in subsequent analyses of all-cause mortality (*1,2*).

When the importance of the H/M threshold of 1.6 in characterizing heart failure patients as being at lower or higher risk of an adverse clinical outcome is considered, reliability of the measurement of this parameter is critical. A fundamental assumption of the ADMIRE-HF trial design was that the H/M ratios measured from images acquired using different clinical nuclear cameras were equivalent as an indicator of the status of the cardiac sympathetic nervous system. The utility of ^{123}I-MIBG cardiac imaging as a routine clinical assessment tool depends on the reliability of H/M ratio determination. Factors that could affect the robustness of planar H/M ratio determinations must therefore be evaluated and quantitatively characterized.

The planar H/M ratio is influenced by several of the physical characteristics of the nuclear γ-camera. Of particular importance is the collimator, in that the amount of attenuator (usually lead) directly affects the measured H/M value. It is well established that medium-energy collimators result in significantly higher H/M values than low-energy, high-resolution (LEHR) collimators (*3–5*). However, even among collimators designated as LEHR by different manufacturers, H/M results for the same patient may differ. This variability may be due to differences in collimator design as well as differences in camera characteristics (e.g., crystal size and thickness, sensitivity) (*6*).

Received May 12, 2017; revision accepted Sep. 5, 2017.
For correspondence or reprints contact: Patrick Cella, GE Healthcare, 100 Results Way, Marlborough, MA 01752.
E-mail: patrick.cella@ge.com
Published online Oct. 17, 2017.

There are 2 primary types of LEHR collimators differentiated by their manufacturing method. Cast-type collimators are created by casting lead as a single piece with spacers inserted in the mold to create the holes perpendicular to the collimator face. Foil-type collimators are created by bending sheets of lead foil and soldering or gluing the junctions between pieces to create the pattern of holes. Cast-type collimators tend to have septa with a slightly higher mean thickness (and are therefore better able to block high-energy photons from ^{123}I) than foil-type collimators, and early foil-type collimators tended to have more defects than more modern foil collimators due to less refined manufacturing methods in the past (*7–10*).

The most efficient and effective means to compare the performance of different imaging equipment such as γ-cameras is with phantoms (*11–14*). These have the advantage of consistency when imaged on different systems, eliminating the variability associated with clinical imaging of different patients on different cameras. An additional advantage of phantoms is that their use involves no radiation exposure to patients. This study used standardized phantoms to assess the intercamera, intracamera, and interhead variability in H/M ratio from planar cardiac ^{123}I-MIBG imaging using commercially available, dual-head γ-cameras. Other groups have used similar phantoms in Japan (*15*) and Europe (*16*) to propose cross-calibrations for camera collimators when calculating the H/M ratio from planar cardiac ^{123}I-MIBG images.

MATERIALS AND METHODS

Phantom

A fillable thorax phantom was developed for use in simulating the typical uptake of ^{123}I-MIBG in the heart, lungs, mediastinum, and a portion of the liver of a patient (Fig. 1A). The thorax phantom was designed to have a nominal H/M ratio of 1.6 when imaged on the Millennium MG (GE Healthcare), the camera used to image the greatest number of subjects in the ADMIRE-HF study (*1*). The H/M value of 1.6 represented the lower limit of normal (mean minus 2 SDs) from published data on control subjects (*17–22*). The phantom consisted of an acrylic block (~45 × 45 cm^2 in size) with a single compartment, with different levels of uptake simulated by cutting flat organs to different depths in the shapes and sizes of planar projections of human adult organs in the thorax and upper abdomen. The structures with higher uptake in humans had a proportionally greater thickness of contained liquid (e.g., mediastinum [0.6 cm], lungs [1.3 cm], heart wall [1.42 cm], and liver [2.4 cm]).

A total of 3 thorax phantoms were produced to enable concurrent tests at different centers, and each phantom was produced on a computer-controlled mill to minimize variability between individual units. The machined acrylic blocks were also checked for tolerances to given specifications using a digital caliper before assembly of the phantoms. Because the phantoms were of single-chamber design, the resulting concentration of activity in each simulated organ was predefined, and no dilution or filling errors could be introduced. The single-chamber design also eliminated potential variability from radioactive decay in between camera measurements because the ratios of activity between simulated organs would remain constant. Finally, acquisitions were specified for a given number of counts, so image quality would remain constant (with acquisition duration as the dependent variable) between phantom measurements, independent of the activity level in the phantom at the time of imaging.

Cameras and Sample Size

Cameras used in the study were manufactured by the 3 companies with the largest number of installed units in the United States and Europe (i.e., GE Healthcare, Philips, and Siemens). Typical models of both standard-field-of-view (FOV) cameras and cardiac-dedicated limited-FOV cameras were selected. All were dual-head cameras capable of 90° configuration for cardiac imaging. Specifications for the LEHR collimators for the cameras are given in Table 1.

The initial sample size calculation was based on an estimate of intracamera variability. Assuming an initially estimated SD of 0.075 for the H/M and a 95% confidence interval (CI) half-length of 0.05, 9 cameras of each model were required to be tested. An interim analysis of data from a single camera model/collimator type combination (GE Healthcare Millennium MG/LEHR) was used to validate the sample size assumptions. This combination was selected as a reference because most subject images in the ADMIRE-HF trial were acquired on the Millennium MG. The measured SD from this analysis was then used to calculate the required sample size for the remainder of the study.

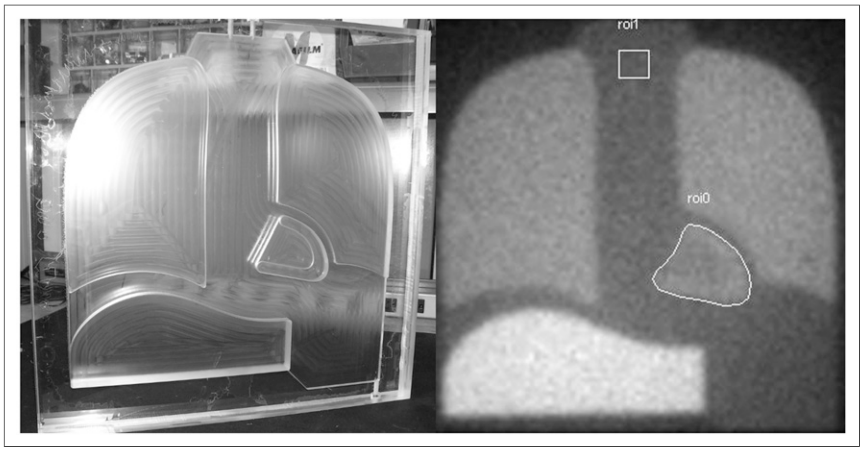

FIGURE 1. Single-chamber ^{123}I-MIBG thorax phantom. Photograph of unfilled phantom (A) and example planar acquisition after filling with ^{123}I (B). Polygonal heart and square mediastinum ROIs of standardized image analysis are shown.

Study Algorithm

Enough imaging centers in the United States were sought to participate to be able to acquire planar phantom images on the required sample size of each camera. The 9 camera models, their collimator types, and number of tested units are summarized in Table 2. If a site had multiple cameras of the models being studied, all available units of those cameras were included, even if the required sample size for that model

TABLE 1
LEHR Collimator Specifications for Studying γ-Cameras

Manufacturer	Model	LEHR collimator type	Mean septal thickness (mm)
GE Healthcare	Millennium MG	Cast	0.20
GE Healthcare	Infinia and Discovery NM series	Foil	0.20
Siemens	e.cam and Symbia	Foil	0.16
ADAC/Philips	Vertex	Foil	0.152 (*26*)
Philips	Brightview	Foil	0.156 (*27*)

had already been achieved. The sites were sent the fillable planar phantom and a source of ^{123}I. In addition, a person from GE Healthcare who was knowledgeable about filling and measuring the phantom was present to ensure adherence to the study protocol. The phantom was imaged by each camera head separately, and the head was positioned anteriorly 5 cm from the phantom surface.

Phantom Preparation and Image Acquisition

For each camera measurement, the phantom was filled with 50–75 MBq of ^{123}I mixed with water and sealed. The phantom was checked for leakage before placing it in the γ-camera.

Within each institution, all cameras included in this study were tested on a single day, without refilling the phantom. For large-FOV cameras, the phantom was centered in the FOV; for small-FOV cameras, all of the heart and as much of the mediastinum as possible were captured in the FOV. Other image acquisition parameters were a static acquisition for a duration of 2×10^6 (i.e., 2 million) counts; matrix, 128×128; pixel depth, 16 bits (word); and energy window, ±10% (or 143–175 keV) with photopeak centered on 159 keV.

Image Analysis

Two imaging technologists were trained on the procedures involved and subsequently performed the analysis of planar images of simulated ^{123}I-MIBG uptake independently of each other. Planar images were analyzed using the Xeleris Workstation (version 2.1; GE Healthcare). The imaging technologists analyzed thorax images by drawing a polygonal region of interest (ROI) around the heart and a 7×7 pixel square ROI in the superior mediastinum region (Fig. 1B). This is the same methodology for ROI size and placement as was used for subject images in the ADMIRE-HF study. H/M was calculated as the ratio of the average counts per pixel of the respective ROIs.

The analysis procedures were repeated for images from each camera head, and results from the analysis of each image were recorded in the case report form.

There was 1 measurement recorded from each of the 2 independent readers on an image obtained from each head of a camera, as well as the average of measurements for readers 1 and 2.

TABLE 2
Summary of Camera Models, Collimator Types, and Sample Size Per Model Included in Study

Camera model	Collimator type	Sample size
GE Healthcare, Millennium MG	LEHR	10
GE Healthcare, Discovery	LEHR	8
GE Healthcare, Infinia	LEHR	10
Philips, Vertex	VXGP/VXHR	8
Siemens, e.cam	LEHR	8
Siemens, Symbia	LEHR	8
Philips, Brightview	LEHR	2
Philips, Cardio 60	LEHR	2
Philips, Cardio MD	LEHR	4

VXGP = vertex general purpose; VXHR = vertex high resolution.

Statistical Analysis

The primary endpoint was intercamera variability in H/M ratio on planar scintigraphy. Data for this endpoint were derived from the image acquired using head 1 (because head 1 is typically used for anterior thorax planar imaging). Assessment of the intercamera variability of the H/M ratio determined for each camera model was based on comparison with the H/M ratio on the prespecified reference camera (Millennium MG). The difference in least-squares means between each camera model and the reference camera was calculated using a mixed model with repeated measures (readers 1 and 2) for which the H/M ratio for the first head tested was the dependent variable and camera model was the independent variable. Only cameras with at least 8 units tested ($n \geq 8$) were included in primary analysis as prespecified in the statistical analysis plan. *P* values of less than 0.05 were considered statistically significant.

Bland–Altman plots were constructed to illustrate the variability in H/M ratio among camera units of the same model and between heads of the same camera unit. Summary statistics were also used to determine intracamera and interhead variability for each camera model.

RESULTS

Interim Analysis

The interim analysis was performed on phantom images from 9 Millennium MG cameras. All images were processed by 1 reader. The SD for the H/M ratio was 0.0713. On the basis this SD, it was determined that 8 cameras of each type would be required to achieve a 95% CI half-length of 0.05. At least 8 examples were then required for each type of camera to be included in the primary analysis.

Cameras Tested

A total of 60 cameras were imaged at 33 different medical centers in the United States. For some of the camera models originally planned to be included at the designated sample size of 8 units (Philips BrightView, Philips Cardio MD, and Philips Cardio 60), it was not possible to have sufficient numbers included within the time frame of the study, due primarily to

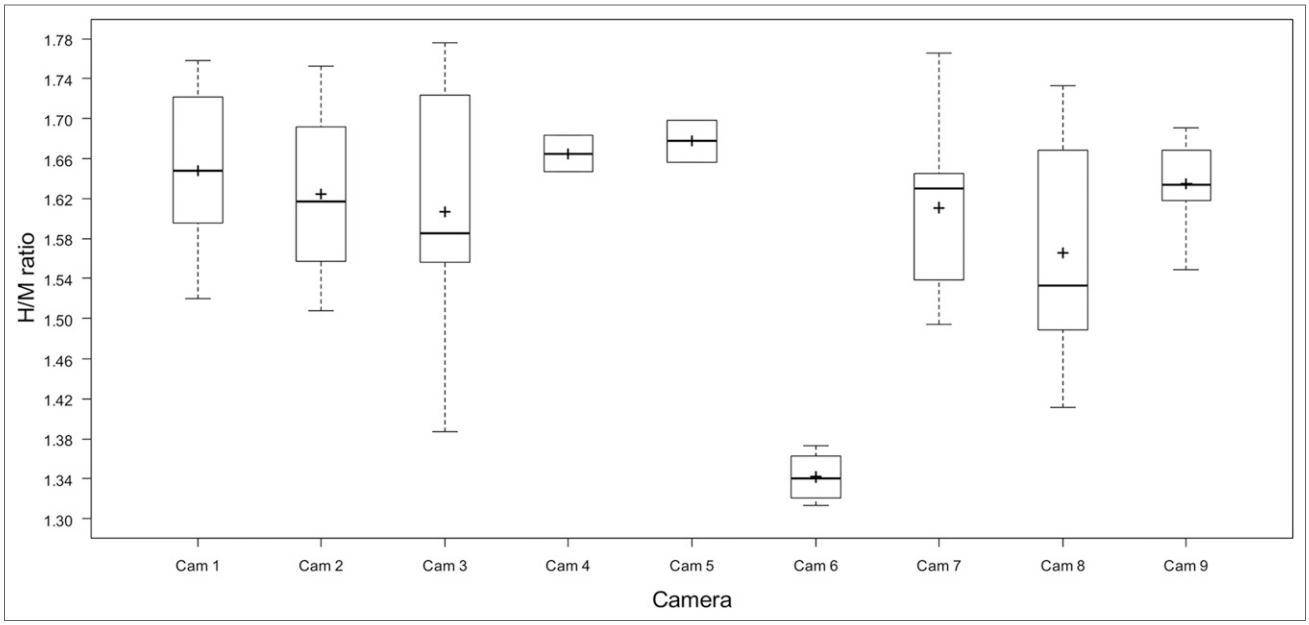

FIGURE 2. Box-and-whisker plot of head 1 H/M ratio. Bottom and top of box are first and third quartiles, respectively. Horizontal line in box is median. + in box represents mean. Ends of the whiskers are minimum and maximum. Cam1 = GE Healthcare Millennium MG/LEHR (n = 10); Cam2 = GE Healthcare Discovery/LEHR (n = 8); Cam3 = GE Healthcare Infinia/LEHR (n = 10); Cam4 = Philips Brightview/LEHR (n = 2); Cam5 = Philips Cardio 60/LEHR (n = 2); Cam6 = Philips Cardio MD/LEHR (n = 4); Cam7 = Philips Vertex/VXGP (vertex general purpose) or VXHR (vertex high resolution) (n = 8); Cam8 = Siemens e.cam/LEHR (n = 8); Cam9 = Siemens Symbia/LEHR (n = 8). VXGP = vertex general purpose; VXHR = vertex high resolution.

difficulty in recruiting imaging centers with the desired cameras and interest in participating. Thus, the following results focus on the 6 camera models with sample sizes of 8 or more.

Image Acquisition

Mean ^{123}I solution activities for each camera ranged from 69.98 to 82.70 MBq, and mean (per-head) acquisition times ranged from 196.8 to 523.5 s.

Inter- and Intracamera Variability

Box plots of H/M ratios (head 1) for all 9 camera models are shown in Figure 2. Mean H/M ratio (head 1) ranged from 1.342 (Philips Cardio MD/LEHR) to 1.677 (Philips Cardio 60/LEHR; Table 3). There was no significant difference in mean H/M ratio between any of the camera models with 8 or more units and the GE Healthcare Millennium MG/LEHR (Table 4). The intracamera variability ($n \geq 8$ units) using head 1 was high, with SDs ranging from 0.0455 (Siemens Symbia/LEHR) to 0.1193 (GE Healthcare Infinia/LEHR) (Table 3).

Interhead Variability

The mean interhead difference of H/M (head 1 minus head 2) ranged from −0.028 (95% CI, −0.090 to 0.033) (Discovery/LEHR) to 0.023 (95% CI, 0.009–0.037) (Siemens e.cam/LEHR). The SD of the interhead difference ranged from 0.017 (difference range, 0.00–0.04) for the e.cam/LEHR to 0.074 (difference range, −0.15 to 0.07) for the Discovery/LEHR. Figure 3 shows the mean H/M ratio (i.e., values for both heads) for each camera plotted against the difference between H/M ratios for head 1 and head 2 as reported by reader 1. Similar results were obtained for reader 2 (data not shown). The plot illustrates the variability in H/M ratio among camera units of the same model and between heads of the same camera.

DISCUSSION

This study assessed the intercamera, intracamera, and interhead variability of H/M ratios from planar images of a thorax phantom containing ^{123}I. The phantom used had a single fillable chamber; thus, the relative ratio of activity in the simulated organs (as well as the H/M) was constant, regardless of the activity level. Hence, the phantom provided a standard for comparing the performance of the different camera models. The H/M value of 1.6 was selected because the same methodology for size and placement of the heart and mediastinum regions on the images as was used for ADMIRE-HF planar images was also used for the present study.

Past research has demonstrated that H/M determinations using a phantom will differ when imaged using γ-cameras and collimators of different types and manufacturers (*3,5,15*). However, our mixed-model, repeated-measures analysis showed no significant difference in mean H/M between 5 camera models (each with $n \geq 8$) and the Millennium MG (the reference camera used for the interim analysis). The mean H/M ratio was within ±0.08 of the nominal phantom H/M value of 1.6 for all 8 large-field camera models. The mean H/M was lower (1.342) for the Cardio MD/LEHR, the

TABLE 3
Analysis of Intracamera Variability in H/M Ratio

Measurement	GE Healthcare, Millennium MG/LEHR (n = 10)	GE Healthcare, Discovery/LEHR (n = 8)	GE Healthcare, Infinia/LEHR (n = 10)	Philips, Brightview/LEHR (n = 2)	Philips, Cardio 60/LEHR (n = 2)	Philips, Cardio MD/LEHR (n = 4)	Philips, Vertex/VXGP or VXHR (n = 8)	Siemens, e.cam/LEHR (n = 8)	Siemens, Symbia/LEHR (n = 8)
Mean ± SD	1.648 ± 0.0776	1.624 ± 0.0849	1.607 ± 0.1193	1.665 (0.0257)	1.677 ± 0.0302	1.342 ± 0.0262	1.611 ± 0.0866	1.566 ± 0.1118	1.635 ± 0.0455
Median	1.65 (range, 1.52–1.76)	1.62 (range, 1.51–1.75)	1.59 (range, 1.39–1.78)	1.66 (range, 1.65–1.68)	1.68 (range, 1.66–1.70)	1.34 (range, 1.31–1.37)	1.63 (range, 1.49–1.77)	1.53 (range, 1.41–1.73)	1.63 (range, 1.55–1.69)
95% CI	1.592–1.703	1.553–1.695	1.521–1.692	1.434–1.895	1.406–1.949	1.300–1.384	1.539–1.683	1.472–1.659	1.597–1.673

Analysis is based on average of H/M ratios from 2 independent readers on camera head 1 for each camera model.
n = sample size for each camera/collimator combination; VXGP = vertex general purpose; VXHR = vertex high resolution.

only limited-field camera in the study. Because the small FOV precluded imaging of the entire phantom, the mediastinum ROI had to be placed more inferior than for the large-FOV cameras, resulting in higher counts per pixel in the ROI (due to greater scatter from heart and lungs) and a lower H/M ratio. Because of the small sample size obtained (n = 4), this camera was not included in the primary analysis.

Although the differences in mean H/M among the large-field camera models were small, the intracamera model variability for the primary analysis cohort ($n \geq 8$) was relatively large. SD ranged from 0.046 for the Symbia/LEHR to between 0.078 and 0.120 for the other 5 camera models. In fact, H/M values for the GE Healthcare Infinia/LEHR (n = 10) ranged from 1.39 to 1.78. One possible explanation for the Symbia/LEHR model producing the lowest SD is that 7 of 8 units tested were located at the same medical center (which presumably uses similar quality control for all of them; the other 5 primary analysis models had units located at 6–9 medical centers).

Nakajima et al. (*15*) found a mean H/M of 1.53 ± 0.07 for acquisitions using ^{123}I in their planar thorax phantom across cameras with LEHR collimators in Japan. The SD calculated was similar to that of most of the large-FOV cameras in the present study. They noted significantly different H/M values in collimators from the same vendor made just a few years apart and supposed that companies routinely modified collimators over time while retaining the same name, which leads to a significant amount of intercamera variability.

Another potential explanation for the high intracamera variability (SD) noted for the older Infinia and e.cam cameras compared with the more modern cameras from each company (Discovery NM 630/670 and Symbia series, respectively) is the use of earlier versions of foil collimators in each. The higher levels of manufacturing defects (susceptible to the high-energy photons of ^{123}I) would result in the higher intracamera H/M SD observed than in the modern cameras using foil collimators or the older camera using cast-type collimators (i.e., Millennium MG).

As anticipated, the SD of the interhead difference was lower than what was observed for intracamera variability. The paired heads within the same γ-camera are manufactured and maintained to be more similar in performance than heads from units of the same model γ-camera.

Although individual cameras of the same and different manufacturers can vary in their performance and the H/M ratios determined from anterior planar images, the fact that the main groups in this study produced comparable mean H/M ratios supports the validity of results from both prospective and retrospective multicenter experiences with ^{123}I-MIBG imaging as a prognostic test for heart failure patients (*1,2,23,24*). Aggregate data from studies including scans from multiple different camera/collimator combinations have consistently demonstrated the same relationship between H/M ratio and prognosis—the lower the H/M ratio (specifically planar H/M lower than 1.6), the poorer the outcome (*1,2,23–25*). Neverthe-

TABLE 4
Analysis of Intercamera Variability of H/M Ratio for Thorax Phantom

Camera/collimator	Sample size	H/M LSM ± SE*	LSM difference ± SE*	*P**
GE Healthcare, Millennium MG/LEHR	10	1.645 ± 0.0286		
GE Healthcare, Discovery/LEHR	8	1.621 ± 0.0319	0.024 ± 0.0429	0.5804
GE Healthcare, Infinia/LEHR	10	1.609 ± 0.0286	0.036 ± 0.0404	0.3824
Philips, Vertex/VXGP or VXHR	8	1.604 ± 0.0319	0.040 ± 0.0429	0.3496
Siemens, e.cam/LEHR	8	1.564 ± 0.0319	0.081 ± 0.0429	0.0655
Siemens, Symbia/LEHR	8	1.631 ± 0.0319	0.014 ± 0.0429	0.7496

*Obtained from mixed model with repeated measures on H/M ratios for first head tested as dependent variable and camera/collimator combination as independent variable. Each camera model is compared with reference camera Millennium MG (GE Healthcare).

LSM = least-squares mean; VXGP = vertex general purpose; VXHR = vertex high resolution.

Only camera/collimator categories with a sample size of at least 8 are included in model, as specified in statistical analysis plan.

less, the present results suggest that for optimal understanding of the significance of an H/M ratio in an individual patient, knowledge of the performance characteristics of the camera/collimator combination on which the ^{123}I-MIBG studied was acquired could be helpful. Although the present study was focused on cameras with LEHR collimators, the use of this or a similar phantom could be employed to study the differences in non-LEHR (e.g., medium energy) collimators.

The intercamera variability in H/M ratios obtained in this thorax phantom study suggests that the imager needs to consider the contribution of his or her particular camera/collimator combination when determining H/M ratios on planar ^{123}I-MIBG images. There are too many variables in the camera and collimator manufacturing, calibration, and maintenance to predict whether an individual camera has a tendency to produce numeric results higher or lower than the average for all camera/collimator combinations of that type. We therefore suggest that the performance of a given camera unit be assessed using an ^{123}I planar phantom before H/M results from ^{123}I-MIBG imaging are used for classifying risk in heart failure patients. Understanding a given camera's performance versus a phantom standard could assist in judging the prognostic significance of clinically borderline H/M ratios (e.g., slightly above or below 1.6).

There are some limitations to the present study. An assessment of the inter- and intrareader variability was not performed to assess any variability introduced by the readers. There was also no record obtained of the calibration and maintenance procedures performed on each camera, as this may have helped to explain some of the variability observed within each camera model. Finally, whereas the mechanical tolerances of the manufactured phantoms were checked within 0.05 in (1.27 mm), a measurement of all 3 phantoms was not performed on the same camera and collimator to confirm equivalence of the measured H/M between them. In the extreme theoretic case that the heart wall chamber was increased by the maximum tolerance in 3 dimensions and the mediastinum chamber thickness was reduced by the maximum tolerance, the net effect on measured H/M would have been as high as 0.11. However, if phantom mechanical tolerances were a significant contributor to the intercamera differences observed, one would have expected to see more clustering of the H/M ratio values into 3 groups (representing the 3 phantoms used for the measurements) and this was not the case.

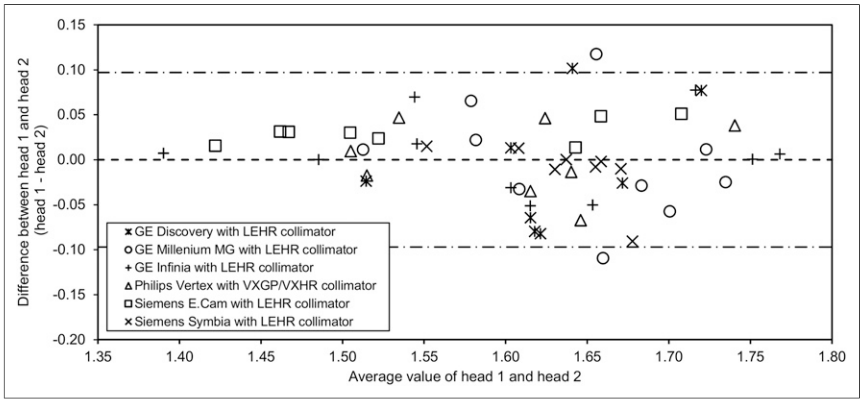

FIGURE 3. Bland–Altman plot for reader 1. Mean H/M (i.e., values for both heads) for each camera is plotted against difference between head 1 H/M and head 2 H/M. Results from reader 2 were similar to those shown here. VXGP = vertex general purpose; VXHR = vertex high resolution.

CONCLUSION

Five commonly used γ-cameras produced mean H/M ratios from simulated ^{123}I-MIBG phantom images that were not significantly different from that obtained by the reference camera model. The mean intercamera variability was also similar to the difference in planar H/M measured in other recent phantom studies using ^{123}I. This finding indicates that the aggregate results of previous clinical trials with ^{123}I-MIBG are valid. However, the results of this study also underscore the importance of testing the

performance of individual cameras against a reference standard before their use in the clinic.

DISCLOSURE

At the time of study conduct, Rikard Owenius was an employee of GE Healthcare. The study was fully sponsored by GE Healthcare. No other potential conflict of interest relevant to this article was reported.

REFERENCES

1. Jacobson AF, Senior R, Cerqueira MD, et al. Myocardial iodine-123 meta-iodobenzylguanidine imaging and cardiac events in heart failure: results of the prospective ADMIRE-HF (AdreView Myocardial Imaging for Risk Evaluation in Heart Failure) study. *J Am Coll Cardiol.* 2010;55:2212–2221.
2. Narula J, Gerson M, Thomas GS, et al. ^{123}I-MIBG imaging for prediction of mortality and potentially fatal events in heart failure: the ADMIRE-HFX study. *J Nucl Med.* 2015;56:1011–1018.
3. Inoue Y, Suzuki A, Shirouzu I, et al. Effect of collimator choice on quantitative assessment of cardiac iodine 123 MIBG uptake. *J Nucl Cardiol.* 2003;10:623–632.
4. Nakajima K, Matsubara K, Ishikawa T, et al. Correction of iodine-123-labeled meta-iodobenzylguanidine uptake with multi-window methods for standardization of the heart-to-mediastinum ratio. *J Nucl Cardiol.* 2007;14:843–851.
5. Verberne HJ, Feenstra C, de Jong WM, et al. Influence of collimator choice and simulated clinical conditions on ^{123}I-MIBG heart/mediastinum ratios: a phantom study. *Eur J Nucl Med Mol Imaging.* 2005;32:1100–1107.
6. Matsuo S, Nakajima K, Okuda K, et al. Standardization of the heart-to-mediastinum ratio of ^{123}I-labelled-metaiodobenzylguanidine uptake using the dual energy window method: feasibility of correction with different camera-collimator combinations. *Eur J Nucl Med Mol Imaging.* 2009;36:560–566.
7. Chang W, Bruch P, Wesolowski C, et al. Performance of cast collimator for SPECT imaging. *J Nucl Med.* 1985;26:44.
8. Gillen GJ, Hilditch TE, Elliott AT. Nonistropic point spread function as a result of collimator design and manufacturing defects. *J Nucl Med.* 1988;29:1096–1100.
9. Gunter DL. Collimator characteristics and design. In: Henkin R, Boyles M, eds. *Nuclear Medicine*, Volume 1. 1st ed. St. Louis, MO: Mosby Publishers; 1996: 96–124.
10. Blend MJ, Patel BA, Rubas D, et al. Foil collimator defects: a comparison with cast collimators. *J Nucl Med Technol.* 1992;20:18–22.
11. Liu CJ, Cheng JS, Chen YC, et al. A performance comparison of novel cadmium-zinc-telluride camera and conventional SPECT/CT using anthropomorphic torso phantom and water bags to simulate soft tissue and breast attenuation. *Ann Nucl Med.* 2015;29:342–350.
12. Penzkofer T, Donandt E, Isfort P, et al. Influence of trigger type, tube voltage and heart rate on calcified plaque imaging in dual source cardiac computed tomography: phantom study. *BMC Med Imaging.* 2014;14:30.
13. Xie X, Willemink MJ, Zhao Y, et al. Inter- and intrascanner variability of pulmonary nodule volumetry on low-dose 64-row CT: an anthropomorphic phantom study. *Br J Radiol.* 2013;86:20130160.
14. Liu YH, Lam PT, Sinusas AJ, et al. Differential effect of 180 degrees and 360 degrees acquisition orbits on the accuracy of SPECT imaging: quantitative evaluation in phantoms. *J Nucl Med.* 2002;43:1115–1124.
15. Nakajima K, Okuda K, Yoshimura M, et al. Multicenter cross-calibration of I-123 metaiodobenzylguanidine heart-to-mediastinum ratios to overcome camera-collimator variations. *J Nucl Cardiol.* 2014;21:970–978.
16. Verschure DO, Poel E, Nakajima K, et al. A European myocardial ^{123}I-mIBG cross-calibration phantom study. *J Nucl Cardiol.* 2017;21:1–7.
17. Cohen-Solal A, Esanu Y, Logeart D, et al. Cardiac metaiodobenzylguanidine uptake in patients with moderate chronic heart failure: relationship with peak oxygen uptake and prognosis. *J Am Coll Cardiol.* 1999;33:759–766.
18. Merlet P, Benvenuti C, Moyse D, et al. Prognostic value of MIBG imaging in idiopathic dilated cardiomyopathy. *J Nucl Med.* 1999;40:917–923.
19. Nakajima K, Taki J, Tonami N, Hisada K. Decreased 123 I-MIBG uptake and increased clearance in various cardiac diseases. *Nucl Med Commun.* 1994;15:317–323.
20. Nakata T, Miyamoto K, Doi A, et al. Cardiac death prediction and impaired cardiac sympathetic innervation assessed by MIBG in patients with failing and nonfailing hearts. *J Nucl Cardiol.* 1998;5:579–590.
21. Parthenakis FI, Prassopoulos VK, Koukouraki SI, et al. Segmental pattern of myocardial sympathetic denervation in idiopathic dilated cardiomyopathy: relationship to regional wall motion and myocardial perfusion abnormalities. *J Nucl Cardiol.* 2002;9:15–22.
22. Suwa M, Otake Y, Moriguchi A, et al. Iodine-123 metaiodobenzylguanidine myocardial scintigraphy for prediction of response to beta-blocker therapy in patients with dilated cardiomyopathy. *Am Heart J.* 1997;133:353–358.
23. Nakata T, Nakajima K, Yamashina S, et al. A pooled analysis of multicenter cohort studies of I-123-MIBG cardiac sympathetic innervation imaging for assessment of long-term prognosis in chronic heart failure. *JACC Cardiovasc Imaging.* 2013;6:772–784.
24. Verschure DO, Veltman CE, Manrique A, et al. For what endpoint does myocardial ^{123}I-MIBG scintigraphy have the greatest prognostic value in patients with heart failure? Results of a pooled individual patient data meta-analysis. *Eur Heart J Cardiovasc Imaging.* 2014;15:996–1003.
25. Agostini D, Verberne HJ, Burchert W, et al. ^{123}I-MIBG myocardial imaging for assessment of risk for a major cardiac event in heart failure patients: insights from a retrospective European multi-center study. *Eur J Nucl Med Mol Imaging.* 2008;35:535–546.
26. Elschot M, Nijsen JF, Dam AJ, et al. Quantitative evaluation of scintillation camera imaging characteristics of isotopes used in liver radioembolization. *PLoS One.* 2011;6:e26174.
27. Philips Brightview SPECT specifications sheet [pamphlet]. Baltimore, MD: Philips Healthcare; 2013.